10400–10413 *Nucleic Acids Research, 2019, Vol. 47, No. 19* *Published online 10 September 2019*
doi: 10.1093/nar/gkz760

Monomeric YoeB toxin retains RNase activity but adopts an obligate dimeric form for thermal stability

Ian J. Pavelich[1,2,3,†], Tatsuya Maehigashi[1,†], Eric D. Hoffer[1,2], Ajchareeya Ruangprasert[1], Stacey J. Miles[1] and Christine M. Dunham[1,2,*]

[1]Department of Biochemistry, Emory University School of Medicine, Atlanta, GA 30322, USA, [2]Emory Antibiotic Resistance Center, Emory University School of Medicine, Atlanta, GA 30322, USA and [3]Department of Chemistry, Emory University, Atlanta, GA 30322, USA

Received June 30, 2019; Revised August 13, 2019; Editorial Decision August 14, 2019; Accepted August 21, 2019

ABSTRACT

Chromosomally-encoded toxin-antitoxin complexes are ubiquitous in bacteria and regulate growth through the release of the toxin component typically in a stress-dependent manner. Type II ribosome-dependent toxins adopt a RelE-family RNase fold and inhibit translation by degrading mRNAs while bound to the ribosome. Here, we present biochemical and structural studies of the *Escherichia coli* YoeB toxin interacting with both a UAA stop and an AAU sense codon in pre- and post-mRNA cleavage states to provide insights into possible mRNA substrate selection. Both mRNAs undergo minimal changes during the cleavage event in contrast to type II ribosome-dependent RelE toxin. Further, the 16S rRNA decoding site nucleotides that monitor the mRNA in the aminoacyl(A) site adopt different orientations depending upon which toxin is present. Although YoeB is a RelE family member, it is the sole ribosome-dependent toxin that is dimeric. We show that engineered monomeric YoeB is active against mRNAs bound to both the small and large subunit. However, the stability of monomeric YoeB is reduced ∼20°C, consistent with potential YoeB activation during heat shock in *E. coli* as previously demonstrated. These data provide a molecular basis for the ability of YoeB to function in response to thermal stress.

INTRODUCTION

Regulation of gene expression through the activation of the SOS, stringent, and heat shock responses during changing environmental conditions is critical for bacterial survival (1–3). These responses generally result in an overall inhibition of cell growth. During the stringent response, inhibition of cell growth occurs by halting gene expression (4). Although originally identified for their role in plasmid maintenance (5–7), toxin-antitoxin complexes are chromosomally encoded and also inhibit growth in response to stress including DNA damage, nutrient starvation, reactive chemical species, heat shock and can aid in the transition to an antibiotic-tolerant or persistent state (8–12). In the past decade, toxin-antitoxin loci have been found to be ubiquitous throughout bacteria and archaea (13). Understanding the regulation and function of toxin-antitoxin complexes in gene expression will unravel their roles in stress responses and thus, antibiotic tolerance.

Toxin–antitoxin pairs are organized into six classes defined by the molecular composition of the toxin and antitoxin components, and how they interact with each other. Type II complexes, in which both the toxin and the antitoxin are proteins, are the best-studied and most abundant systems (reviewed in (12)). During nutrient-rich growth, the expression of toxin–antitoxin pairs is regulated via a negative feedback loop where the DNA-binding antitoxin binds at operator regions that overlap with its promoter region. Toxin and antitoxin proteins form tightly associating complexes and, in some cases, different toxin and antitoxin stoichiometric levels can regulate optimal transcriptional repression (14–16). Stress causes antitoxin proteolysis by cellular proteases, releasing its cognate toxin to inhibit downstream cellular targets. Although two type II toxins inactivate DNA gyrase (17,18), the majority inhibit protein synthesis and RNA metabolism by degrading messenger RNAs, transfer RNAs, ribosomal RNA, or by modification of tRNAs, aminoacyl synthetases or elongation factors (19–30). It is not clear why type II toxins predominately target protein synthesis. However, given the enormous cellular resources devoted to translational regulation in bacteria, one hypothesis is that inhibition of translation may represent a facile mechanism to respond quickly to environmental changes (4).

A subclass of type II toxins that disrupt translation are ribosome-dependent RNases (for review see (12,31)).

*To whom correspondence should be addressed. Tel: +1 404 712 1756; Fax: +1 404 727 2738; Email: christine.m.dunham@emory.edu
†The authors wish it to be known that, in their opinion, the first two authors should be regarded as Joint First Authors.

Ribosome-dependent toxins are small proteins (∼8–13 kDa) that adopt a conserved microbial RNase-fold containing a concave active site and are members of the RelE superfamily including *Escherichia* coli RelE, YafQ, YoeB, and *Proteus vulgaris* HigB (32–36). These RNases degrade mRNAs actively undergoing translation on the ribosome, specifically within the aminoacyl (A) site, the same site where tRNA binds to the ribosome to interact with mRNA codons for decoding. To date, most of these toxins only target the coding regions of mRNAs and can recognize both sense and stop codons but not AUG start codons (20,37–39). HigB and YafQ toxins primarily target codons that are commonly found after the AUG start codon suggesting they may interfere with the initiation phase of translation (38,40–42). Although ribosome-dependent toxins share a common RNase fold representing the larger RelE superfamily, their sequence identities are extremely low, which makes them difficult to identify. Specifically, active site residues are highly variable which may give rise to markedly different substrate preferences and thus, by extension, may allow the degradation of different mRNA codons. The structure of RelE bound to the 70S along with *in vitro* functional assays suggest a substrate preference of the CAG glutamine codon and stop codons (preference of UAG > UAA > UGA) (20,33) (all codons shown in the 5′-3′ direction). Additional studies suggest a wider range of mRNAs targeted by RelE with a N–R–R codon preference, where N and R indicate any nucleotide and purines, respectively (43). In contrast, HigB prefers an adenosine at the third nucleotide position in the codon while YafQ seems to only recognize an AAA lysine codon (37,40,41). Similar to the broad codon specificity of RelE, YoeB cleaves UAA stop and AAA lysine codons (39,44), but can also recognize AAU asparagine, CUG leucine, GCG alanine, and GCU alanine codons (45). In the 70S-YoeB structure solved with a UAA stop codon in a pre-cleavage state, the preference for N-R-R codons was rationalized by how YoeB interacts with its mRNA substrate (46), although this contradicts the wide range of codons YoeB can cleave (39,45). During our structural comparison of the HigB toxin bound to the 70S ribosome with the 70S-RelE and 70S-YoeB structures, we identified that the mRNA was incorrectly modeled in the 70S-YoeB structure potentially obscuring key details about YoeB codon recognition (46). We remodeled the mRNA in unbiased electron density to better understand how YoeB recognizes the UAA codon (41). While the remodeling of mRNA provided some insights into the comparison of YoeB with other ribosome-dependent toxins, outstanding questions remain including how YoeB recognizes sense codons and whether YoeB influences the mRNA position after cleavage.

RelE superfamily members are typically monomeric proteins whether in the apo form, bound to its cognate antitoxin, or when bound to the ribosome (33,35,36,41). However, YoeB binds to the 70S ribosome as a dimer but the biological relevance of this oligomeric state remained unclear (46). Additionally, how YoeB recognizes different codons and whether significant conformational changes occur post cleavage is unknown. Here, we examine YoeB bound to both the UAA stop codon and asparagine AAU sense codon in pre- and post-cleavage states on the ribosome. Our results indicate that YoeB has loose overall codon specificity but makes specific interactions with the mRNA codon possibly for optimal mRNA cleavage. Furthermore, to test the requirements of the YoeB dimer, we engineer a YoeB monomer and test for activity either with mRNA positioned on the 30S subunit or the 70S. We demonstrate that the YoeB monomer retains activity confirming the YoeB dimer is not required for function. Interestingly, we find that the engineered monomeric YoeB is ∼20°C less stable than the wild-type YoeB dimer, consistent with YoeB being the only type II toxin activated during thermal stress, thus providing a molecular basis for its action (47).

MATERIALS AND METHODS

Strains and plasmids

The *E. coli* strains BL21 Gold (DE3) pLysS (F^- *ompT* *hsdS*(r_B^- m_B^-) *dcm*$^+$ Tet^r *gal* λ(DE3) *endA* Hte [pLysS Cam^r]) (Agilent/Stratagene) was used for the purification of YefM, YoeB and YoeB variant proteins. Plasmids used in this study are listed in Supplementary Table S1. The pET21c-*yefM-yoeB* was a generous gift from Professor Masayori Inouye (Robert Wood Johnson Medical School, NJ, USA).

Purification of YefM, YoeB and YoeB variants

BL21 Gold (DE3) pLysS cells containing pET21c-*yefM-yoeB* were grown in lysogeny broth (LB) medium supplemented with 200 μg/ml ampicillin at 37°C to an OD_{600} of 0.5–0.7 and induced with 0.4 mM IPTG. Cultures were grown for 3 h before harvesting cells by centrifugation at 3500 × *g* for 30 min. Cell pellets were resuspended in lysis buffer containing 20 mM Tris–HCl pH 7.5, 250 mM KCl, 0.1% Triton X-100, 5 mM β-mercaptoethanol, 0.1 mM phenylmethylsulfonyl fluoride and 0.1 mM benzamidine. Cells were lysed by sonication and centrifuged at 20 000 × *g* for 30 min to obtain the supernatant containing the YefM–YoeB$(His)_6$ complex. Cleared lysate was applied to a HisTrap FF Crude^{TM} Ni^{2+}-Sepharose column (GE Healthcare) pre-equilibrated with binding buffer containing 40 mM Tris–HCl pH 7.5, 250 mM KCl, 20 mM imidazole, 5 mM $MgCl_2$, 10% glycerol and 5 mM β-mercaptoethanol. After the lysate was loaded, the column was washed for an additional 20 column volumes with the same buffer.

For wild-type YoeB and YefM purification, denaturing buffer containing binding buffer plus 6 M guanidine-HCl was applied for 15 column volumes to denature the bound YoeB–YefM complex to elute YefM. Elution fractions containing denatured YefM were combined, shock refolded by rapid dilution into binding buffer followed by filtration using 0.45 μm steriflip (Millipore). YefM was applied to a Superdex 75 SEC column (GE Healthcare) in a buffer containing 40 mM Tris–HCl pH 7.5, 250 mM KCl, 5 mM $MgCl_2$ and 5 mM β-mercaptoethanol. Denatured YoeB$(His)_6$ was refolded on the Ni^{2+}column by slowly removing guanidine-HCl in 20 column volumes and >8 hrs. YoeB$(His)_6$ was eluted in a buffer containing 300 mM imidazole. Fractions containing YoeB$(His)_6$ were combined and applied to Superdex 75 SEC column in the same buffer as YefM.

For monomer YoeB W5A and W5A/W10A variants purifications, cleared lysate was applied to a HisTrap FF

Crude™ Ni^{2+} sepharose column (GE Healthcare) and washed as described above, however, reduced guanidine–HCl (2 M) was applied to partially disrupt the YefM–YoeB complex, followed by gradual removal of guanidine-HCl from the column. Bound proteins (YefM-YoeB and free YoeB mix) were then eluted from the column by applying elution buffer containing 300 mM imidazole. The later fractions containing mostly free YoeB mutant, judged by SDS-PAGE, were applied to Superdex 75 SEC column (GE Healthcare) to further purify the monomeric YoeB.

The purity of all proteins was determined to be >95% by SDS-PAGE analysis and their concentrations were determined by the Bradford assay (Biorad). Purified proteins were divided into ∼10 μl aliquots, flash froze in liquid nitrogen, and stored at −80°C until further use.

In vitro mRNA cleavage assays

Escherichia coli 30S and 70S were purified from MRE600 cells as previously described (40,42). Purified *E. coli* 30S or 70S (1.2 μM) were programmed with 5′- [^{32}P]-labeled mRNA (0.6 μM; 5′-GCCAAGGAGGUAAA AAUGAAUCAGA-3′ or 5′-GCCAAGGAGGUAAAAA UGUAACAGA-3′) at 37°C for 6 min in 50 mM KCl, 10 mM NH_4Cl, 10 mM $Mg(OAc)_2$ and 5 mM HEPES, pH 7.5. *E. coli* $tRNA^{fMet}$ (3 μM; Chemical Block) was incubated for 30 min while YoeB (0.6 μM) was incubated for 10 min at 37°C, followed by incubation at room temperature for additional 20 min. The reaction was stopped by the addition of formamide loading dye and incubation at 65°C for 2 min. Reactions were resolved on a 18% polyacrylamide-8M Urea gel, the gel dried and exposed to a phosphoimager. Cleavage activities were quantified with ImageQuant TL™ (GE Healthcare) using the 1D gel analysis function to compare the cleavage band intensities across all lanes. Two technical replicates of the *in vitro* cleavage assays were performed.

Thermus thermophilus 30S complex formation and crystallization

30S subunits were purified, crystallized, and cryoprotected as has been previously described (48). The mRNAs were chemically synthesized (ThermoFisher, Dharmacon) with the sequence 5′-AAU AAA-3′ with AAU representing the A-site codon (Supplementary Table S2). After cryoprotection, 100 μM mRNA and 220 μM YoeB were soaked into empty 30S crystals for at least 12 hrs. Crystals were flash cooled by plunging into liquid nitrogen and stored for data collection.

Thermus thermophilus 70S complex formation, crystallization and structure determination

70S ribosomes were purified as previously described (49). Complex formation was performed as described for the mRNA cleavage assay. Four x-ray datasets were collected at the Northeastern Collaborative Access Team (NE-CAT) 24-ID-C facility at the Advanced Photon Source at Argonne National Laboratory (Argonne, IL). These datasets included the 3.7 Å-structure of the 30S bound to YoeB, the 3.2 Å-structure of the 70S bound to YoeB with a non-cleavable mRNA (pre-cleavage state with an A-site AAU codon), the 3.1 Å-structure of the 70S bound to YoeB with mRNA (post-cleavage state with an A-site AAU codon), and the 3.5 Å-structure of the 70S bound to YoeB with mRNA (post-cleavage state with an A-site UAA codon). The post-cleavage state structures were obtained by incubating 70S-YoeB complexes with a 25-nucleotide mRNA similar to the *in vitro* cleavage assays. The mRNA is cleaved during the crystallization trials as seen previously for the 70S-RelE and 70S-HigB structures (33,41). A total of 45° of data with 0.2° oscillations (30S-YoeB) and 90° of data with 0.15° oscillations (70S-YoeB) were collected on a PILATUS pixel 6M-F detector (DECTRIS Ltd., Switzerland) using 0.972 or 0.9795 Å radiation, respectively (Supplementary Table S3). Data were integrated and scaled using the program XDS (50) and molecular replacement was performed using the PHENIX software suite (51). Iterative rounds of refinement in PHENIX and model building were performed using the program Coot (52).

For the 30S-YoeB dataset, the structure was solved by molecular replacement using PDB code 1J5E as the search model (53). An initial round of refinement was performed with each ribosomal subunit defined as a rigid group, followed by coordinate and grouped ADP refinement (per residue) with ten rigid groups determined by TLS server (54). $F_o - F_c$ electron density maps indicated that the YoeB dimer was positioned in the A site (Supplementary Figure S1). Each monomer of the YoeB dimer model from the PDB code 4V8X (46) was rigid docked. Individual refinement of the RNA coordinates was performed with tight restraints. Final refinement of the structures including YoeB gave crystallographic $R_{work}/R_{free} = 20.6/22.4\%$. Residues 1–84 of the YoeB in direct contact with the decoding center (denoted as $YoeB^a$) and residues 1–84 on the second YoeB ($YoeB^b$) were built.

The 70S structures were solved by molecular replacement using PDB code 4V6F as the search model with mRNA and tRNA ligands removed (55). In each 70S-YoeB structure, F_o-F_c electron density maps show an unambiguous signal for mRNA, P-site $tRNA^{fMet}$ and the YoeB dimer in the A site. YoeB was initially docked in the A site using the previous YoeB structure solved in the absence of the ribosome to avoid any bias in the modeling (PDB code 2A6S) (32). In particular, YoeB residues that interact with mRNA (Glu46, Arg59, Glu62, Arg65, His83 and His84) were extensively remodeled to fit the $F_o - F_c$ difference density. Iterative rounds of refinement in PHENIX and model building in Coot were performed (51,52). These unbiased maps allowed modeling of both mRNA and YoeB. The final YoeB model was built for residues 1–84 for both YoeB monomers (Supplementary Figure S1).

Site-directed mutagenesis

The plasmid pBAD33-*yoeB* and pET21c-*yefM-yoeB* were kind gifts from Professor Masayori Inouye (Robert Wood Johnson Medical School, NJ, USA) and served as templates for site-directed mutagenesis using the QuikChange Lightning Kit (Agilent). Primers are shown in Supplementary Table S4.

Differential scanning fluorimetry

Purified wild-type YoeB, YoeB W5A or YoeB W5A/W10A variants (5 μM) were used in the DSF experiments. SYPRO Orange dye (Invitrogen) was added at a 1:1000 dilution. Reactions were heated at a rate of 0.5°C per min, using a StepOne Plus Real Time PCR system (ThermoFisher) and fluorescence was recorded using the ROX filter (602 nm). Data were analyzed by normalizing fluorescence and then fitting the curves using the Boltzmann equation to determine the melting temperature (T_m) (GraphPad Prism, version 8.0.2). Non-linear regression fitting to a Boltzmann sigmoidal curve was performed to determine the T_m of each sample. A one-way ANOVA was performed with Dunnett post-hoc analysis ($n = 2$, $F = 1234$, $df = 5$, $P \leq 0.0001$). The T_m of wild-type YoeB is significantly different as compared to the YoeB W5A and YoeB W5A/W10A variants (mean difference of 20.6°C and 21.1°C respectively, adjusted $P = <0.0001$). Experiments were performed in triplicate with two independent replicates for each variant.

RESULTS

YoeB cleaves mRNA bound to both the 30S subunit and the 70S

YoeB cleaves both sense and stop codons (39,45) and has been shown to associate with free 50S and 70S albeit in the absence of mRNA (39,45). Given that mRNA is located on the 30S subunit in the mRNA path, it is currently unclear how the toxin interacts with the large subunit. Indeed, although the *P. vulgaris* HigB also appears to bind to the 50S in polysome profiles (38), HigB can cleave mRNA bound to only the small subunit (42). Considering that YoeB cleaves sense codons (39,44,45), we reasoned that YoeB may also recognize a 30S initiation-like complex. To test this possibility, we performed in vitro mRNA cleavage assays where we incubated purified wild-type YoeB with the *E. coli* 30S or 70S ribosome programmed with a 25-nucleotide mRNA and *E. coli* $tRNA^{fMet}$ in the peptidyl(P) site of the ribosome. When YoeB binds to the 70S, both an asparagine AAU sense and a UAA stop codon are cleaved to form a product that runs on a denaturing gel at ∼19 nucleotides as compared to standards (Figure 1A). RNAs containing a 3′ phosphate typically run 1–2 nucleotides faster than 3′ dephosphorylated RNAs (56). Since YoeB-mediated cleavage resulted in mRNA containing a 3′ phosphate (46), we hypothesize that our cleavage product means YoeB cleaves the phosphodiester backbone between the second and third nucleotide of the A-site codon (between nucleotides 20 and 21 in our mRNA) consistent with previous results (39). We also found that YoeB cleaves mRNA bound to the 30S (Figure 1A). However, YoeB is unable to cleave the mRNA to completion on the 30S subunit similar to HigB toxin mRNA cleavage on the 30S (42). In addition, another mRNA product is observed indicating that YoeB can cleave the mRNA at two different locations when bound to the 30S. Possibilities for this include that the mRNA moves in the context of the 30S or that in the absence of the 50S, both YoeB monomers are needed for its optimal positioning to cleave the mRNA codon.

Molecular recognition of the 30S subunit by the YoeB dimer

Our biochemical results above indicate that YoeB can cleave mRNA bound to the 30S in contrast to polysome profiles that showed YoeB did not bind the 30S subunit (39,45). To understand the molecular basis of the interaction of YoeB with 30S and mRNA, we next solved a 3.8-Å X-ray crystal structure of the complex (Supplementary Table S1 and Figure 1B). *Thermus thermophilus* 30S subunits were purified and crystallized as previously described (48) and a short six nucleotide mRNA and purified wild-type YoeB were soaked into preformed 30S crystals. The mRNA contains an A-site AAU asparagine codon containing 2′-*O*-methyl (2′-OMe) modifications at all three A-site positions to prevent cleavage. $2F_o - F_c$ electron density maps clearly show that YoeB interacts with the 30S subunit as a dimer (Figure 1B and Supplementary Figure S1A). Unfortunately, the mRNA is not visible which is similar to the 30S-HigB structure we previously solved (42). One possible reason for this is that in the 30S crystal lattice, the 3′ end of the 16S rRNA and the 16S rRNA spur from an adjacent molecule in the asymmetric unit mimic a P-site codon and anticodon stem–loop, respectively. As we previously suggested, the absence of the P-site tRNA and mRNA codon may prevent the binding of the small mRNA in the A site (42). Nonetheless, this structure provides insights into how the dimeric YoeB toxin recognizes the small subunit.

Monomeric *E. coli* YoeB is a 10.2 kDa protein and forms a compact globular structure consisting of a five-stranded β-sheet and two α-helices (32). Consistent with the way the 70S-YoeB structure was previously described (46), the YoeB monomer closest to the mRNA path is referred to as $YoeB^a$ and the more distant monomer as $YoeB^b$. In general, the YoeB dimer occupies the A site between the 30S head and the body domains (Figure 1B). The binding site of $YoeB^a$ overlaps completely with that of the anticodon stem-loop of the tRNA and $YoeB^a$ also interacts with the shoulder domain of the 30S subunit (Figures 1B and 2). The position of $YoeB^b$ does not overlap with where tRNA binds and instead packs against the 30S head domain, contacting 16S rRNA helix 31 (h31) (Figure 1B and D). The overall YoeB dimer arrangement on the 30S is similar to when bound to the 70S (46) with a root mean-square deviation (r.m.s.d.) of 1.2 Å, for 168 equivalent Cα atoms (84 residues in each YoeB chain). Additionally, YoeB, in the context of the 30S-YoeB structure, is similar to the structure of YoeB in the $YefM_2$-YoeB toxin-antitoxin complex as well as to the previously determined 70S-YoeB structure (r.m.s.d. = 1.5–1.6 Å) (32).

Although α-helix 2 (α2) in each YoeB monomer is enriched with basic residues that theoretically could interact with the negatively charged backbone of 16S rRNA, only $YoeB^a$ makes extensive interactions with the ribosome (Figure 1C). $YoeB^a$ contacts the 30S head and body domains via 16S rRNA helix 18 (h18) and helix 44 (h44), respectively. Residue Arg22 is within hydrogen bonding distance to the phosphate backbone oxygens of nucleotide U531 in h18. Weak electrostatic interactions are formed between $YoeB^a$ residues Lys26 and Gly43 with the phosphate backbone oxygens of C519 while Lys42 contacts the 2′-OH of C519 (Figure 1C). In contrast, $YoeB^b$ makes weak interactions

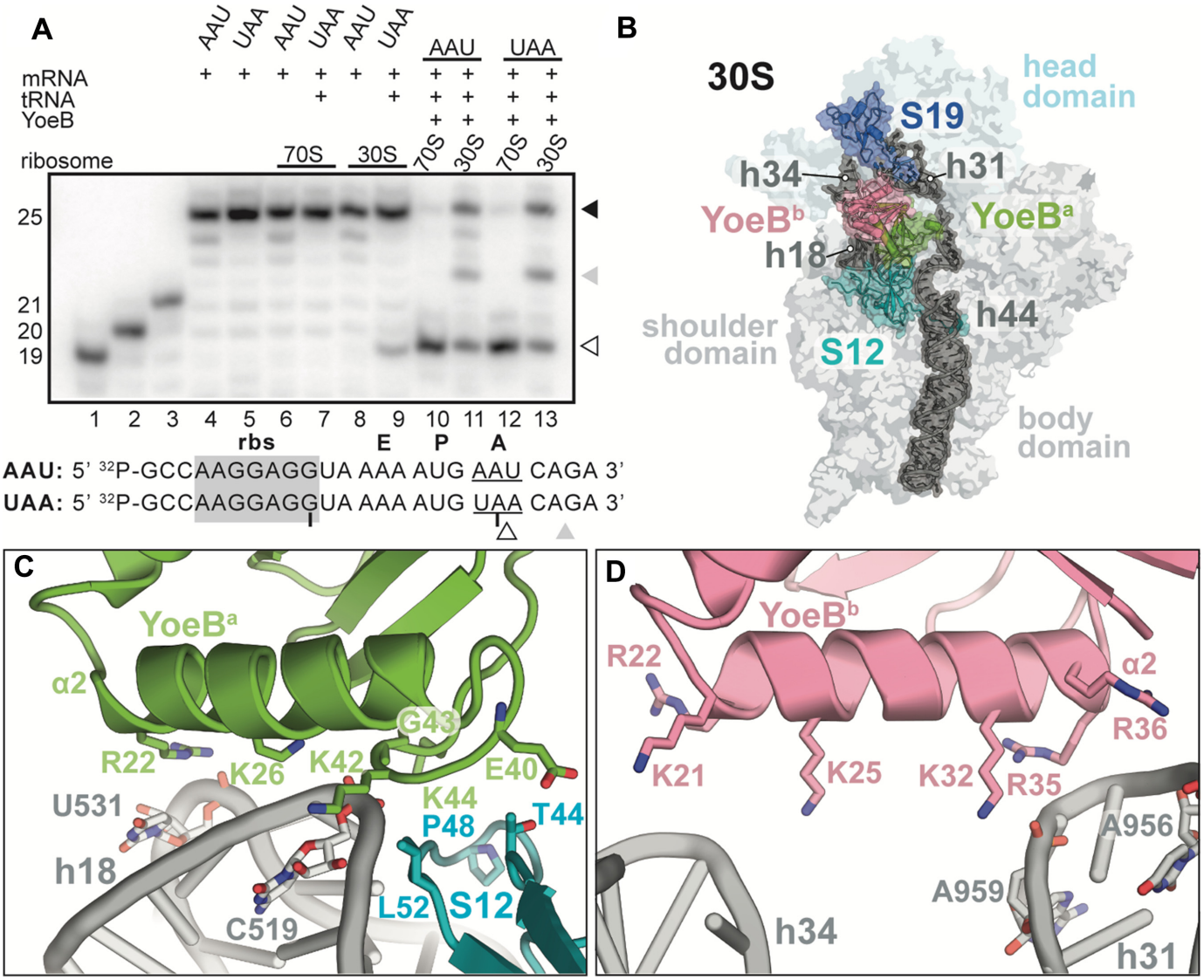

Figure 1. *E. coli* YoeB recognizes the 30S A site. (**A**) *In vitro* cleavage assays of ^{32}P-5′-labeled mRNA bound to either a 70S or 30S programmed with P-site tRNA^{fMet}. The mRNA sequence contains a ribosome binding site (rbs) and E-, P- and A-site codons are shown above the mRNA sequence (tick lines are shown for every 10 nucleotides). The A-site codons contained either an AAU asparagine or UAA stop codon. Ribosome complexes were formed as described in the Methods section. YoeB was incubated for 10 mins and reactions were quenched and monitored by denaturing PAGE. Both codons are cleaved by YoeB when bound to a 30S and 70S complex (lanes 10–13). Cleavage on the 30S occurs to a lesser extent and an extra band is observed (lanes 11 and 13). Full length mRNA is denoted by a closed arrowhead, cleavage product by an open arrowhead and the extra mRNA band by a gray arrowhead. Neither codon is cleaved in the absence of YoeB (lanes 6–9). 19-, 20- and 25-nucleotide mRNA standards and AAU and UAA containing mRNAs are shown for comparison (lanes 1–5). (**B**) A 3.7 Å-structure of *Thermus thermophilus* 30S-YoeB where YoeB binds in the A site as a dimer between the head, body and shoulder domains. The YoeB monomer closest to the mRNA path is shown in green (YoeB^{a}) while the distal YoeB monomer is shown in pink (YoeB^{b}). 16S rRNA helices (h18, h31, h34, and h44) and proteins (S12, S19) that YoeB interacts with are indicated in dark gray and blue, respectively. (**C**) YoeB^{a} interactions with 16S rRNA h18 and S12 of the 30S. (**D**) YoeB^{b} makes weak electrostatic interactions with 16S rRNA h34 and h31.

with the 16S rRNA located in the 30S head domain (Figure 1D). YoeB^{b} residues Lys21, Arg22 and Lys25 are adjacent to the backbone of 16S rRNA h34 but likely only form weak electrostatic interactions (>3.5 Å). Additional weak electrostatic interactions are made between YoeB residues Lys32, Arg35 and Arg36 with helix 31 (h31) of the head domain of the 30S. Although ribosomal S12 residues Glu40 and Lys44 interact with YoeB bound to the 70S (46), in the context of the 30S, YoeB slightly shifts away from S12 thus ablating these interactions.

Molecular mechanism of YoeB recognition of a UAA stop codon

YoeB cleaves AAA lysine, AAU asparagine, UAA stop, CUG leucine and GCG alanine codons on the ribosome in the A site (39). As previously described, a structure of the 70S with YoeB bound to an A-site UAA stop codon in a pre-cleavage state contained an incorrect modeling of the mRNA (46). To directly compare how ribosome-dependent toxins RelE, HigB and YoeB interact with their mRNA substrates on the ribosome, we rebuilt and refined

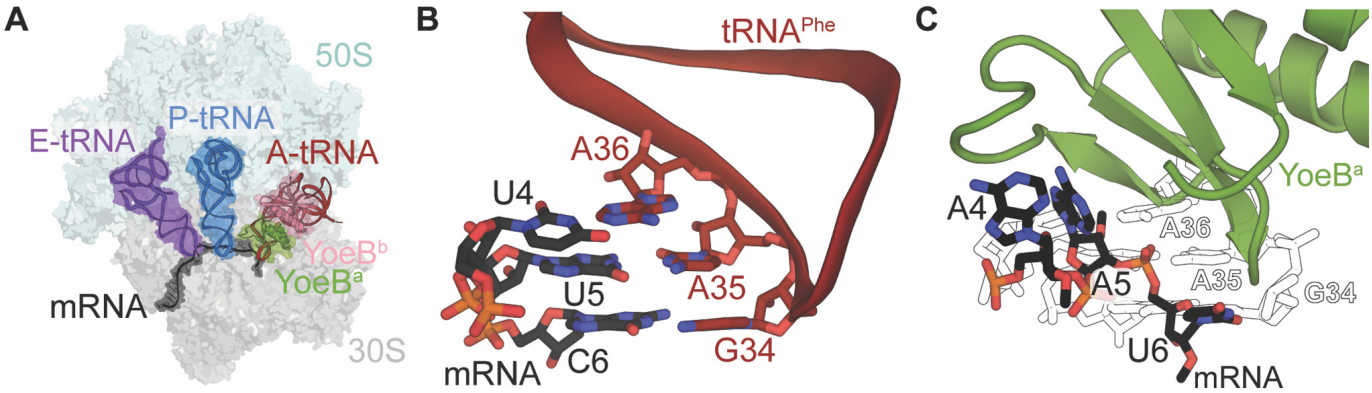

Figure 2 YoeB binds in the A site normally occupied by A-site tRNA. (**A**) View of the *Thermus thermophilus* 70S ribosome with dimeric YoeB bound in a UAA post-cleavage state. 50S and 30S subunits are shown as background and A-, P- and E-site tRNAs are shown in red, blue and purple, respectively. The YoeB monomer closest to the mRNA path is shown in green (YoeB^{a}). The YoeB dimer overlaps with the position of A-tRNA^{Phe} (PDB code 4V5l). (**B**) tRNA^{Phe} interaction with its cognate mRNA codon in the A site. (**C**) The mRNA (black) is re-positioned for cleavage by YoeB^{a} as compared to the normal anticodon stem loop and mRNA pairing from (**B**) shown in outline.

the mRNA into unbiased electron density (41). We found that YoeB induces a similar conformation of the A-site codon as compared to the RelE and HigB toxin (33,41). The rebuilt mRNA indicates that YoeB conserved residues Glu46, Lys49 and Asn51 interact with the first (U4) and the second (A5) nucleotides of the mRNA within the A site (Figure 3A) (mRNA numbering starts with +1 in the P site with A-site nucleotides numbered 4–6). Although this structure provided insights into how the YoeB dimer interacted with the 70S in a pre-cleavage state, how YoeB interacted with a UAA stop codon after mRNA cleavage was necessary to determine which YoeB residues are important for activity. For example, HigB residues move considerably after mRNA cleavage and pre- and post-cleavage structures provided significant insights into its mechanism (41). Therefore, we solved a 3.5-Å x-ray crystal structure of 70S bound to YoeB and mRNA containing an A-site UAA stop codon that undergoes cleavage during the crystallization process (Figure 3, Supplementary Figure S1D and Supplementary Table S1). The post-cleavage state was solved using unmodified 25-mer mRNA and cleavage was indicated by a lack of electron density for the third nucleotide (A6) of the A-site codon (Supplementary Figure S2). In both pre- and post-cleavage states of YoeB bound to an UAA stop codon, YoeB adopts an almost identical conformation with an r.m.s.d. of 1.2 Å for equivalent 168 Cα atoms (84 residues in each YoeB chain). Although the YoeB dimer appeared to colocalize with both the 70S or 50S subunit in polysome profile assays (39) but not the 30S subunit, there are no interactions between YoeB and the 50S subunit in this structure (Supplementary Figure S3).

When bacterial toxins bind to the A site of the ribosome to cleave the mRNA phosphodiester backbone, the mRNA is dramatically pulled into the toxin active site (33,41) (Supplementary Figure S4). Upon YoeB binding to the A-site codon, we find that the mRNA is similarly pulled into the YoeB active site in slight contrast to what was previously published (41,46). In the pre-cleavage state, the side chain amine group of YoeB^{a} residue Asn51 forms a π-π stacking interaction with the nucleobase of first nucleotide of the A-site codon U4 (Figure 3A). Given the nonspecific nature of this interaction, it appears that any nucleotide could be accommodated at this position consistent with primer extension analysis of mRNAs cleaved by YoeB (45). In contrast to the absence of interactions with the first nucleotide position of the codon, YoeB^{a} surrounds the second and third A-site nucleotides (Figure 3A). In the incorrect build of A5 (46), it appears there are base-specific interactions with the sidechains of highly conserved YoeB^{a} residues Arg59, Arg65 and Tyr84. However, in our rebuild, Arg65 and Tyr84 are too distant to interact with A5, however, Arg65 interacts with the scissile phosphate and the O4′ of the ribose of A6 (Figure 3A). Interactions with the second A5 nucleotide not observed in the previous 70S-YoeB structure include the interaction of Glu46 with the 2′-OH and the base-specific interaction of Lys49 (Figure 3A). The sidechain of Glu46 forms a hydrogen bond with the 2′-OH of A5 and the backbone oxygen and amine groups of Lys49 form hydrogen bonds with the Hoogsteen face of A5 that adopts a *syn* conformation. Only cytosine in an *anti* confirmation can fulfill this hydrogen bonding pattern (Supplementary Figure S5). At the third nucleotide position of the A-site codon (A6), YoeB^{a} residues Glu63 and His83 (β4) stack with the A6 nucleobase. A6 undergoes a 180° rotation around its phosphate backbone as compared to when tRNA is present, where its nucleobase forms stabilizing stacking interactions with His83 and Glu63 (Figure 3B).

Upon mRNA cleavage by YoeB, the position of U4 and A5 minimally changes however, YoeB^{a} moves slightly away from the mRNA path. This movement results in an ablation of the stacking and the hydrogen bonding interactions between Asn51 and U4 and Glu46 with the 2′-OH of A5 (Figure 3B). The formation of the 3′-phosphate positions YoeB^{a} residues Arg59, Arg65, and Tyr84 within hydrogen bonding distance (Figure 3B and C). Together, these two structures indicate that while any nucleotide can be accommodated in the first position, the hydrogen bonding network formed between the second position (A5) and stacking interactions at

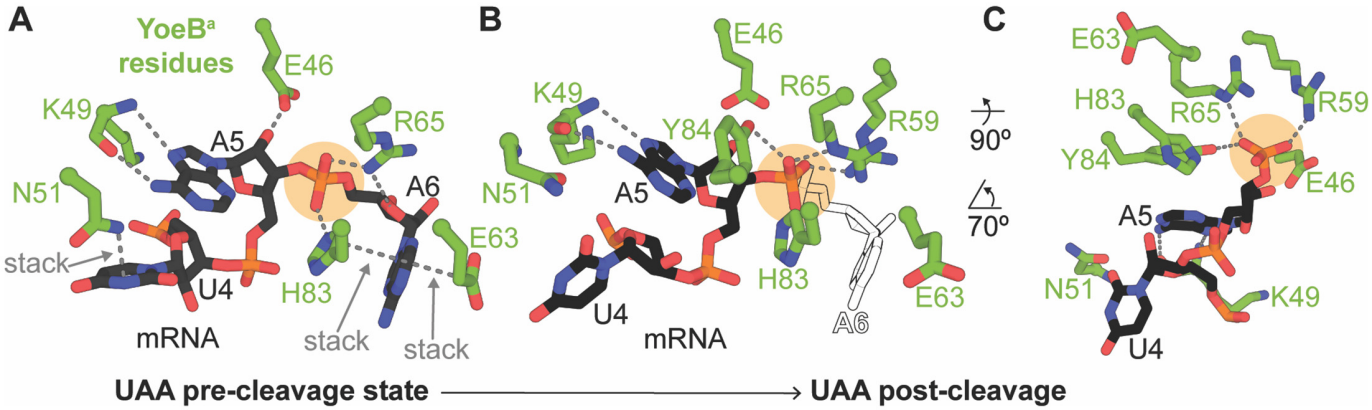

Figure 3. The influence of YoeB on the mRNA path when bound to an UAA stop codon. (**A**) Our remodel of the interactions between the A-site UAA stop codon and YoeB in a pre-cleavage state (PDB code 4V8X, remodeled). The scissile phosphate is highlighted in orange. (**B**) In a post-cleavage state (PDB code 6OXI, this study), interactions between the A-site UAA stop codon and YoeB. The position of the cleaved A6 is shown in outline for comparison. (**C**) Upon cleavage, Arg59, Arg65 and Tyr84 interact with the 3′-phosphate.

the third position (A6) with YoeB residues seem to impose some constraints on which nucleotides would be a good YoeB substrate.

Molecular mechanism of YoeB recognition of a AAU asparagine sense codon

YoeB also cleaves the AAU sense codon in addition to the UAA stop codon (39,45). Given that YoeB^a appears to select for the UAA stop codon by extensive interactions with the third nucleotide (Figure 3A), and these two codons differ at this third position, we solved x-ray crystal structures of 70S-YoeB bound to a 25-mer mRNA containing an A-site AAU codon in a pre- and post-cleavage states to 3.2 and 3.1 Å, respectively (Figure 4, Supplementary Figure S1C, S1D, and Supplementary Table S1). In these structures with the AAU codon, the first nucleotide in the codon is positioned closer to the P-site tRNA enabling interactions between the ribose O4′ atom of nucleotide 36 and the N6 atom of U4 but the stacking interaction between Asn51 and U4 is no longer observed (Figures 3A and 4A). In both UAA and AAU codons, there is an adenosine at the second nucleotide position. In the two 70S-YoeB structures, there is conservation in how YoeB interacts with A5 suggesting that differences in the codon do not change how YoeB recognizes the nucleotide at the second position. At the third position, substitution of an adenine with an uridine still causes a reorientation of the nucleobase towards the mRNA path, however, U6 does not stack between Glu63 and His83 (Figure 4A and Supplementary Figure S6). In the post-cleavage state, YoeB^a residues Arg59 and Tyr84 move towards the mRNA to hydrogen bond with the newly formed 3′ phosphate while Arg65 maintains interactions with the phosphate (Figure 4B and C). These interactions were previously observed (46). Together, these structures suggest that while purines stack more efficiently with the third nucleotide of the A-site codon upon YoeB binding, this interaction is not essential considering that YoeB still cleaves codons containing pyrimidines at the third position.

YoeB-induced conformational changes of the decoding center

When tRNA binds to the 70S A site, the mRNA-tRNA pair is monitored by 16S rRNA nucleotides and ribosomal protein S12 in the decoding center (57). During this decoding process, 16S rRNA nucleotides G530, A1492 and A1493 monitor the codon-anticodon interaction to determine if the interaction is cognate. A1492 and A1493 flip from an internal loop in 16S rRNA h44 to probe for Watson-Crick base-pairing at the first and second positions of the codon–anticodon interaction. At the same time, G530 moves inward to form a single hydrogen bond with A1492 and flips from a *syn* to an *anti* conformation to interact with the second and third codon positions. Additionally, the entire 30S shoulder domain moves inward towards the intersubunit space of the A site and these conformational changes collectively contribute to tRNA selection (58,59). YoeB binding also induces similar conformational rearrangements of 16S rRNA nucleotides however, there are slight differences as compared to the process of tRNA selection. In the structure of the pre-cleavage 70S bound to a UAA stop codon, binding of YoeB causes A1492 and A1493 to flip out of h44 to interact with mRNA and YoeB residues Glu46, Pro47 and Lys49, as previously seen (46). Although A1913 of 23S rRNA Helix 69 (H69) moves during tRNA decoding to interact with A1492, upon YoeB binding, the position of A1913 remains constant because YoeB^a binding occupies this space (Figure 5B). However, in the post-cleavage state, A1492 rotates ∼150° back into h44 (Figure 5C). This movement places A1492 adjacent to A1913 where it partially stacks with A1913 ablating interactions with YoeB^a. In both pre and post-cleavage states, YoeB binding inserts Lys44 (of the α2–β2 loop) and Arg59 (β2) residues between G530 and A1492 thus preventing interactions between these two nucleotides that are usually required for correct tRNA selection (Supplementary Figure S7). These interactions with the decoding nucleotides are preserved in the 70S structures bound to the AAU sense codon.

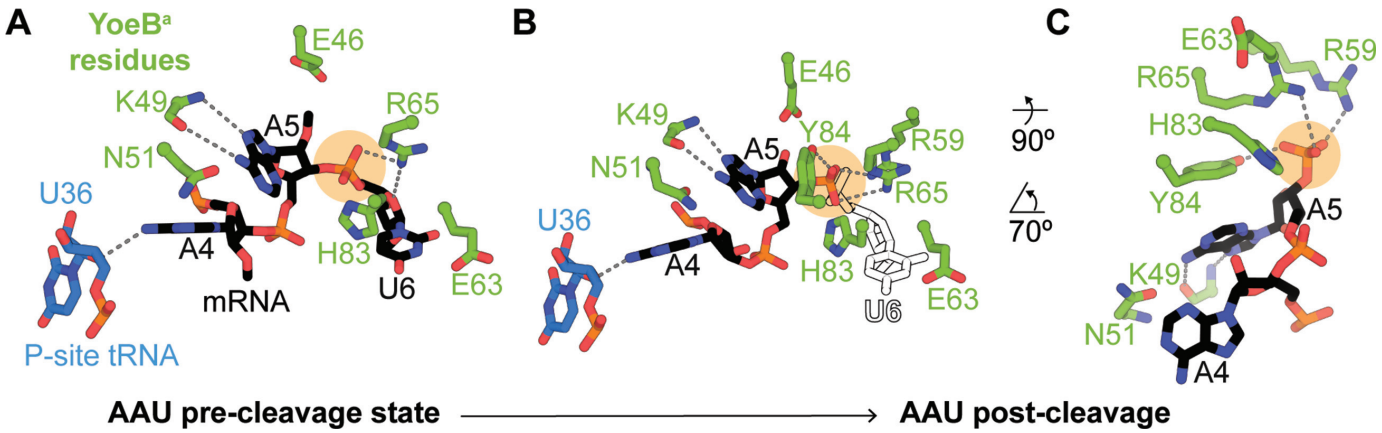

Figure 4. The influence of YoeB on the mRNA path when bound to an AAU sense codon. (**A**) Interactions between YoeB residues and the A-site AAU asparagine codon in a pre-cleavage state. The scissile phosphate is highlighted in orange (PDB code 6OXA). (**B**) In a post-cleavage state (PDB code 6OTR), interactions between YoeB residues and the A-site asparagine codon. The position of the cleaved U6 is shown in outline for comparison. (**C**) Upon YoeB-mediated cleavage, Arg59, Arg65 and Tyr84 interact with the phosphate.

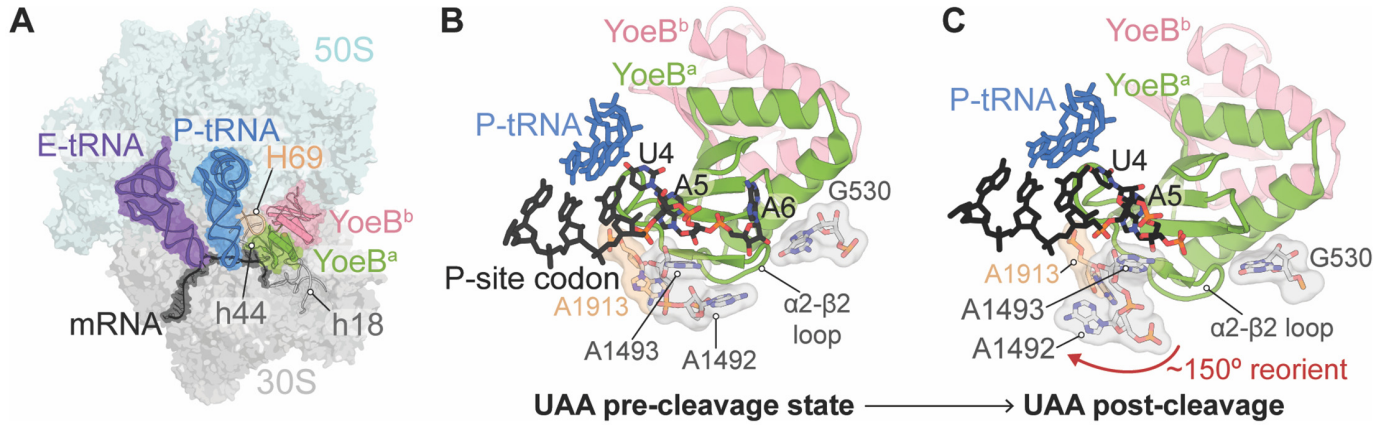

Figure 5. The influence of YoeB on the mRNA path when bound to a UAA stop codon. (**A**) Structure of dimeric YoeB bound to the *Thermus thermophilus* 70S ribosome. Color scheme is the same as in Figure 1. YoeB^a interacts with 16S rRNA helices h18 and h44 (gray) and 23S rRNA helix H69 (gold) adjacent to the mRNA path (black). P- and E-site tRNAs are shown as blue and purple, respectively. (**B**) YoeB^a interacts with the A-site decoding center when bound to a UAA stop codon in a pre-cleavage state (by the inclusion of 2′-OCH_3 at all three A-site nucleotides) solved by Feng *et al.* (46). All three A-site nucleotides (U4, A5, A6) are shown in black, and are monitored by 16S rRNA nucleotides A1492, A1493, and G530 of h44 (gray) and 23S rRNA A1913 (gold). We rebuilt the mRNA as previously published (41). The P-site mRNA codon (black) and anticodon nucleotide (blue) are shown for perspective. (**C**) A 70S-YoeB post-cleavage state where the α2-β2 loop of YoeB prevents A1492 forming hydrogen bonds with G530.

Monomeric YoeB retains ribosome-dependent ribonuclease activity yet is thermally unstable

Our data presented here and the previous YoeB structure bound to the ribosome demonstrate that YoeB binds to both the 30S and 70S as a dimer (46). The YoeB dimer interface is formed by hydrophobic surfaces of α1 and α2 from each YoeB monomer and a hydrogen bonding network between residues Glu7, Tyr13, Gln17, Asn28 and Arg35 (Figure 6A and Supplementary Figure S8). Two tryptophan residues, Trp5 and Trp10, form a hydrophobic pocket and are also involved in the formation of the YefM-YoeB toxin-antitoxin complex via interactions with C-terminal residues of YoeB (32). Since all known ribosome-dependent toxins are monomers including RelE, YafQ and HigB (33,36,40,41,60), it is unclear why YoeB adopts a dimeric form. To test whether a YoeB monomer retains RNase activity, we introduced alanine mutations of W5A and W5A/W10A in an attempt to disrupt the tryptophan cluster and thus engineer a YoeB monomer. Wild-type YoeB dimer elutes as a compact dimer at ∼16 kDa as determined by size exclusion chromatography (SEC) while the apparent molecular weight of both purified YoeB W5A and YoeB W5A/W10A is ∼11 kDa indicating that YoeB is a monomer (Figure 6B).

We next tested whether YoeB W5A and YoeB W5A/W10A variants cleave mRNA in the context of 30S and 70S ribosomes using the in vitro cleavage assay previously described. Both YoeB variants cleave AAU and UAA codons on the 70S to near completion similar to wild-type YoeB (Figure 6C and Supplementary Figure S9). In the context of the 30S subunit, the YoeB W5A and YoeB W5A/W10A variants cleave AAU and UAA codons on mRNA to ∼55 and 65% completion, respectively as compared to ∼80% on the 70S ribosome (Figures 1A and 6C). However, YoeB variants do not produce an additional

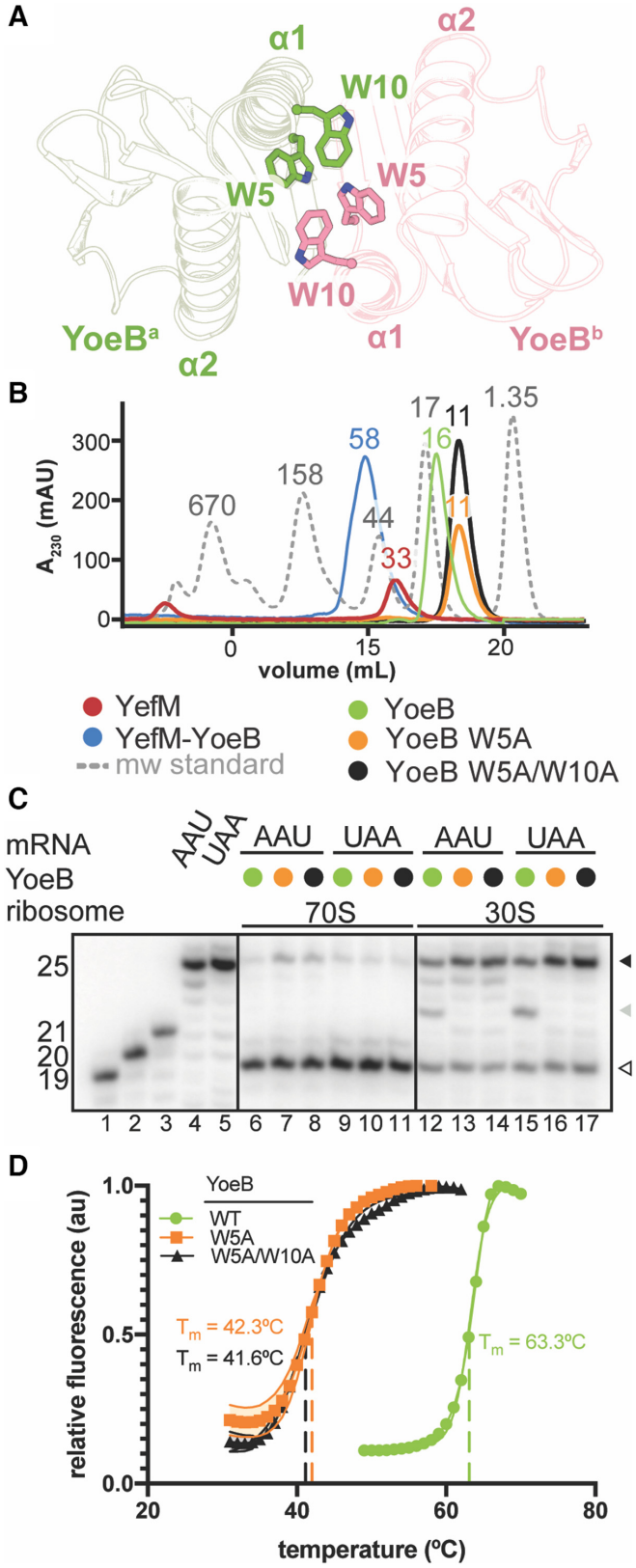

Figure 6. Monomeric YoeB is active but is less thermal stable. (**A**) YoeB residues W5 and W10 of each YoeB monomer comprise the dimer interface and were selected for mutagenesis experiments to create a monomeric YoeB. (**B**) Size exclusion chromatography of purified YoeB, YefM-YoeB, and YoeB variants indicating that the W5A and W5A/W10A variants are monomeric. The number above each peak denotes the molecular weight in kDa. Approximate molecular weights of YefM, YefM-YoeB, and YoeB are 27.9 kDa, 59.6 kDa, and 22.4 kDa, respectively. YoeB variants W5A and W5A/W10A elute at ∼11 kDa. (**C**) *In vitro* cleavage assays of ^{32}P-5′-labeled mRNA bound to either a 70S or 30S programmed with P-site tRNA^{fMet}. The mRNA sequence used in these assays is the same as in Figure 1A. Both mRNAs are cleaved by YoeB when bound to a 30S and 70S complex. YoeB variants W5A and W5A/W10A are both active in cleaving mRNA bound to either the 30S or 70S as compared to wild-type YoeB. Full length mRNA is denoted by a closed arrowhead, cleavage product by an open arrowhead and the extra mRNA band by a gray arrowhead.19-, 20- and 25-mer mRNA standards and AAU and UAA containing mRNAs are shown for comparison (lanes 1–5). The line separating the gels indicates each region of the figure were taken from different parts of a single gel. (**D**) DSF assays demonstrate that wild-type YoeB (green, T_m = 63.3°C) is more thermostable than YoeB variants W5A (orange, T_m = 42.3°C) or W5A/W10A (black, T_m = 41.6°C). Fluorescence values were normalized to the highest tested temperature and the boundary of each line represents the mean ± SD of values of three independent experiments.

cleavage band on the 30S in contrast to wild-type YoeB cleavage on the 30S subunit (Figures 1A and 6C). It is not clear the exact reason for the disappearance of this extra band when YoeB is monomeric but it may indicate that YoeB^b affects the position of YoeB^a and this somehow prevents the movement of mRNA that produces an extra mRNA cleavage band (Figure 1A). These data indicate that an engineered YoeB monomer can cleave ribosome-bound mRNA and somehow this oligomeric state influences the position of the mRNA in the context of the 30S only.

YoeB is activated during thermal stress (47) and therefore we wondered whether one role of a YoeB dimer is for thermal stability. To test this, we performed differential scanning fluorescence (DSF) experiments of wild-type YoeB, YoeB W5A and YoeB W5A/W10A proteins. Wild-type YoeB has a melting temperature (T_m) of 63.3°C while the YoeB W5A and YoeB W5A/W10A variants are ∼20°C less stable (Figure 6D). These data suggest that the YoeB dimer is stabilized and active during thermal stress consistent with data from the Hayes group (47).

DISCUSSION

In this study, we focus on understanding the mechanism of action of the type II toxin, YoeB. YoeB is an endonuclease that cleaves mRNA bound to the ribosome but only in the A site, the site where tRNAs are brought to the ribosome for decoding of the mRNA codon. We find that YoeB is capable of cleaving mRNA codons on both the 30S and 70S ribosomes suggesting that interactions with the 50S are not required for YoeB activity. We further solved an x-ray crystal structure of YoeB bound to the 30S, revealing extensive interactions of YoeB^a with the decoding center while YoeB^b minimally interacts with the 30S. Given that YoeB can cleave codons immediately downstream of the AUG start codon in a subset of mRNA tested (39), our results indicate that YoeB targets mRNAs even during the initiation phase of translation before recruitment of the 50S. Although YoeB is active as a dimer, our experiments show that a dimeric oligomeric state is not essential for cleavage of the mRNA by YoeB. Instead, YoeB likely forms a dimer to persist during thermal stress in which it is upregulated (47).

Traditional RNases, including type II ribosome-dependent toxins, display a wide range of substrate specificity. As with other type II toxins, YoeB cleaves between the second and third nucleotide of the mRNA codon presented in the A site and appears to target a range of codons most commonly at the beginning of the coding region or at stop codons (39,46). The previously reported structure of YoeB bound to a 70S containing an A-site UAA stop codon in a pre-cleavage state suggested that any nucleotide could be accommodated at the first nucleotide position of the codon due to a lack of base-specific interactions (46). Although this structure provided insights into potential YoeB mRNA specificity, the mRNA was incorrectly modeled as we previously discussed upon comparison with type II HigB toxin bound to the 70S ribosome (41). This prompted us to rebuild the mRNA and examine how YoeB interacts with its mRNA substrate. Here, we further extend these studies to determine how YoeB residues change after mRNA cleavage of the UAA stop codon and additionally how YoeB cleaves the sense UAA codon. In the rebuild, YoeB^{a} Lys49 makes nucleobase-specific interactions that define which nucleotide is allowed at the second position of the codon while Glu46 stabilizes the nucleotide by interactions with its 2′-OH (Figure 3A). It is clear that cytosine can make similar interactions as adenosine if it adopts an *anti* conformation, which is similar to how HigB recognizes A and C codons at this second position (41). YoeB^{a} residues Arg65 and His83 interact with the scissile phosphate while Glu63 and His83 stack with A6 or the third nucleotide of the codon (Figure 3). A post-cleavage state reveals that Arg65 maintains interactions with the 3′-phosphate and Arg59 moves towards the 3′-phosphate, both events likely important in stabilizing the transition state of the reaction. These structures begin to provide insights into the mechanism of YoeB cleavage of mRNA.

To extend our understanding of potential codon specificity by YoeB, we also solved structures in both the pre-and post-cleavage states bound to an AAU sense codon. Interestingly, A4 contacts the P-site tRNA at nucleotide 36 unlike when an uridine is present at this first position (Figure 4A and B). Regardless, clearly this is not an important interaction as all four nucleotides are found at the first position in codons cleaved by YoeB (39,44). Interactions of YoeB^{a} residue Lys49 with A5 are preserved in both UAA and AAU codons bound to the 70S providing evidence that the identity of surrounding nucleotides, that is, the first and third nucleotides in the codon, do not alter how the second nucleotide is pulled from the mRNA path to present the scissile phosphate for cleavage (Figures 3 and 4). Modeling of other nucleotides at the second position indicates that while a cytosine may be accommodated, either a guanosine or uridine would not maintain this hydrogen-binding pattern (Supplementary Figure S5), consistent with *in vivo* cleavage assays (32,39,44). At the third nucleotide position, although A6 in the UAA structure is clearly stabilized by stacking interactions with Glu63 and His83, this stacking is ablated when A6 is substituted with U6. YoeB mediated mRNA cleavage assays indicate YoeB can cleave codons containing a guanine at this position, suggesting there may be subtle nucleotide specificity at this third position (45) (Figures 3A, 4A, and Supplementary Figure S6). This is consistent with previous observations that the majority of nucleobases recognized by YoeB in the third position are purines (32,39,44,45). Overall, these data provide accumulating evidence that YoeB has loose codon specificity.

The 30S decoding center undergoes conformational rearrangements regardless of when tRNAs or translation factors bind and this includes when type II toxins RelE, HigB and YoeB bind (33,41,46). Surprisingly, ribosome-dependent toxins induce slightly different conformational changes of the decoding center that may be reflective of how such stalled ribosome complexes are recycled after toxin departure (Figure 7). During decoding, 16S rRNA nucleotides A1492, A1493 and G530 along with S12 residues monitor mRNA-tRNA interactions and concurrently, the 30S adopts a closed state resulting in the shoulder domain moving towards the A site. Comparison of pre- and post-cleavage states induced by RelE reveals that the decoding center changes very little (Figure 7C and D) (33). 16S rRNA nucleotide A1492 is pulled from h44, G530 moves to a *syn* conformation, however, A1493 remains stacked with A1913. The absence of A1493 movement towards G530 indicates that this is not a fully closed state. Toxin HigB also induces an incomplete closing of the A site but there are differences between pre- and post-cleavage states (Figure 7E and F) (41). For example, upon HigB binding but before mRNA cleavage has occurred, A1492 rather than A1493, partially stacks with A1913. After cleavage by HigB, A1492 moves ∼45° away from A1913. Interestingly, YoeB induces changes that are distinct from changes induced by either RelE or HigB (Figures 5, 7A and B). In the pre-cleavage state with YoeB bound, both A1492 and A1493 are flipped from h44 and G530 adopts a *syn* conformation, all changes that reflect a closed state (Figure 7A). After cleavage, A1492 flips back into h44 however, it does not stack with A1913 (Figure 7B). In all 70S structures containing the three toxins, A1492 is prevented from interacting with G530 by a toxin loop that functions as a physical barrier to prevent the ribosome adopting fully closed states. The differences that toxins exert upon the A-site may be due to their physical size and surrounding electrostatic interactions (Supplementary Figure S10). RelE and HigB proteins are slightly smaller than the monomeric YoeB, but more importantly, YoeB occupies more space in the A site to more fully interact with A1492, A1493 and A1913 (Supplementary Figure S10D). Additionally, this extended position of YoeB may be aided by the surrounding negative electrostatic surface of the 50S in relation to the distal YoeB^{b} monomer (Supplementary Figure S10E). For example, there is only one point of opposing charges between the 50S and YoeB^{b} that could potentially result in repelling YoeB^{b} from the 50S surface towards the A site (Supplementary Figure S4 and S10E). This repelling may result in YoeB^{b} somehow influencing the position of YoeB^{a} important for interactions with the codon. Support for this includes the additional mRNA cleavage band in cleavage assays with only the 30S that then is ablated when engineered monomeric YoeB is tested. Thus, the dimeric state of YoeB may account for the more closed state of the A site as compared to RelE and HigB (Figure 7).

What are the consequences of the binding of toxin that induce different conformations of A-site decoding nu-

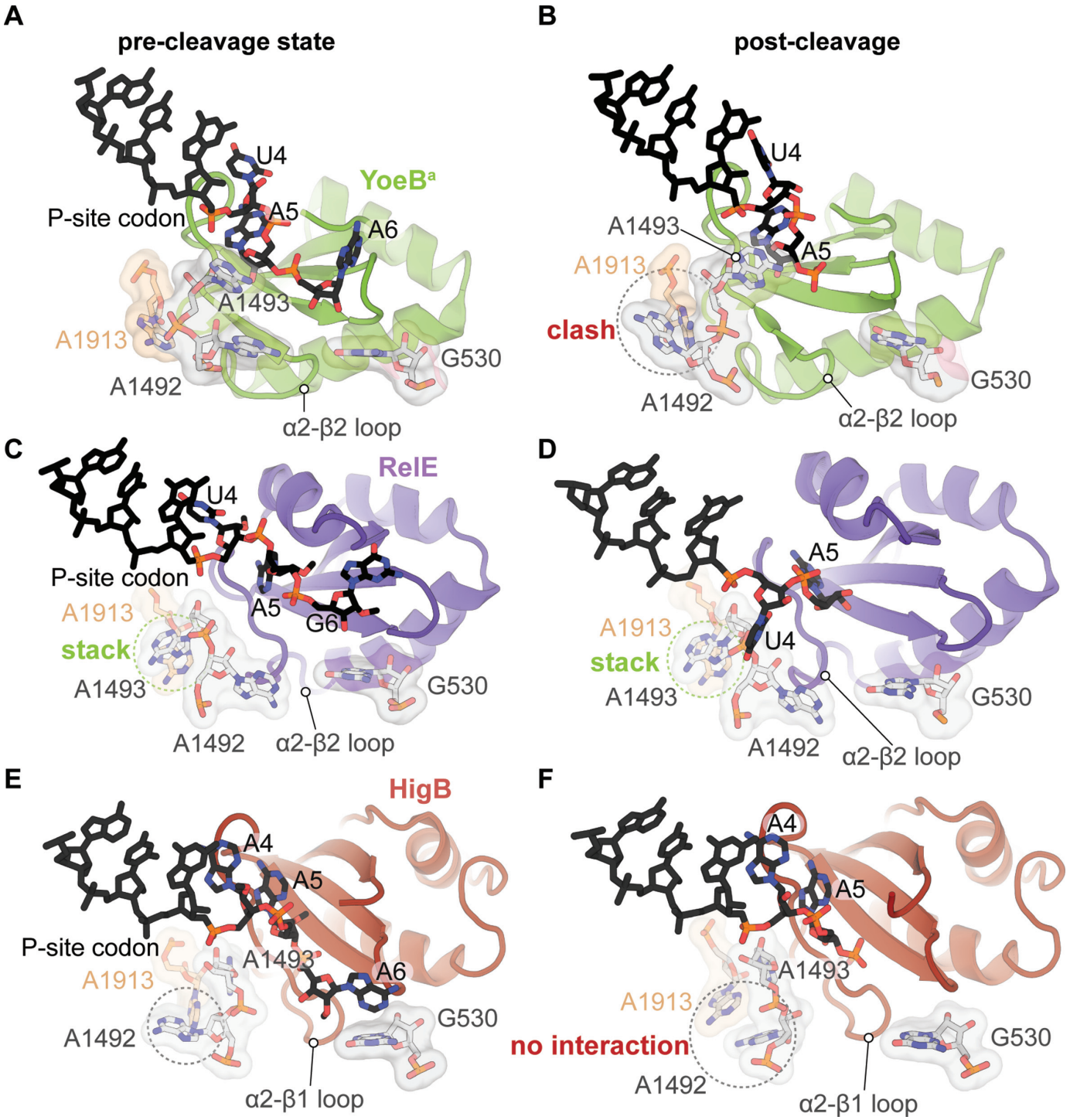

Figure 7. Comparison of the influence of YoeB, RelE and HigB toxins on the mRNA path. (**A**) Interaction of YoeB with the A-site decoding center bound to a UAA stop codon in a pre-cleavage state is shown (PDB code 4V8X, remodeled). All three A-site nucleotides (U4, A5, A6) are monitored by 16S rRNA A1492, A1493, and G530, and 23S rRNA A1913. (**B**) Interaction of YoeB with the A-site decoding center bound to a UAA stop codon in a post-cleavage state is shown (PDB code 6OXI, this study). Reorientation of A1492 post-cleavage results in a clash with A1913 of H69. (**C**) Interaction of RelE with the A-site decoding center bound to a UAG stop codon in a pre-cleavage state is shown (33). All three A-site nucleotides (U4, A5, G6; black) are monitored by 16S rRNA A1492, A1493, and G530 and 23S rRNA A1913. (**D**) Interaction of RelE with the A-site decoding center bound to a UAG stop codon in a post-cleavage state is shown (33). There is little to no significant conformational changes between the two states. In both cases, the RelE α2-β2 loop prevents A1492 from forming hydrogen bonds with G530. (**E**) Interaction of HigB with the A-site decoding center bound to a AAA lysine codon in a pre-cleavage state is shown (41). All three A-site nucleotides (A4, A5, A6) are monitored by 16S rRNA A1492, A1493, and G530, and 23S rRNA A1913. In this state, A1492 only partially interacts with A1913. (**F**) Interactions of HigB with the A-site decoding center bound to a AAA lysine codon in a post-cleavage state is shown (41). In this state, A1492 moves away from and no longer stacks with A1913. In both cases, the HigB α2-β2 loop prevents A1492 from forming hydrogen bonds with G530.

cleotides? One possibility is that variations of open and closed states could influence toxin release after cleavage. For example, toxins that remain bound to the ribosomes post cleavage could, in addition to the inhibition of translation, also protect ribosomes that are queued on mRNAs from other toxins that cleave rRNA such as *E. coli* MazF, *M. tuberculosis* MazF-mt6 and MazF-mt9 (61–64). In addition to protection, toxin-bound ribosomes would also prevent ribosome recycling. Conversely, other toxins that rapidly dissociate from the ribosome would have the opportunity to cleave many mRNAs thus inhibiting translation to a larger extent. In line with this argument, toxins such as RelE and YoeB that appear to have loose specificity may help combat nutritional deficiencies arising from stress by targeting the majority of transcripts to promote recycling of nascent chains to help replenish nutrients such as amino acids. Future studies aimed at understanding the steps after toxin RNase activity would provide important insights into these downstream events.

The question of why YoeB is a dimer while all other structurally-homologous, ribosome-dependent toxins are monomers motivated us to test whether the dimeric form is related to its activity. Engineered monomeric YoeB appears to be as active as the wild-type YoeB dimer indicating the dimeric state is not a requirement for function. Recent studies by the Hayes group demonstrate YoeB is the sole ribosome-dependent toxin that cleaves mRNA during elevated temperatures in *E. coli* (47). These cleaved mRNAs are then recognized by tmRNA-SmpB, ArfA, or ArfB for the release of the nascent chain required for the recycling of ribosomes. Consistent with these data, the YoeB dimer is more thermal stable than the YoeB monomer rationalizing why YoeB has evolved to be dimeric during heat shock (Figure 6D).

Expression of type II toxin-antitoxin systems is typically regulated via a negative feedback loop where stress attenuates antitoxin proteolysis leading to transcriptional derepression. Whether specific stresses activate different toxins is unknown, however, it has been shown that nutritional stress causes rapid activation of *E. coli* RelBE, MazEF, HicAB, YafNO, YgiNM, and YgiUT toxin-antitoxin complexes (23) while other systems may be regulated by the SOS response (*E. coli* YafQ-DinJ) (37), antibiotics (*P. vulgaris* HigB) (65) and more recently, thermal stress (*E. coli* YoeB-YefM) (47). While traditional RNases monitor whether mRNAs are functional, these toxins serve more as a stress-specific mechanism of translational inhibition. Many outstanding questions remain regarding the activation, regulation and downstream effects of toxins on bacterial physiology, however, our mechanistic insights into YoeB activity expands our understanding of ribosome-dependent toxins activated during thermal stress.

DATA AVAILABILITY

Coordinates and structure factors were deposited in Protein Data Bank under accession codes 6NY6, 6OXA, 6OTR, 6OXI.

SUPPLEMENTARY DATA

Supplementary Data are available at NAR Online.

ACKNOWLEDGEMENTS

We thank Dr. Graeme Conn and Dunham lab members Ha An Nguyen and Pooja Srinivas for critical reading of the manuscript. We additionally thank Rachel Erdmann, Jhomar Marquez and Eduardo Sanabria for technical support.

FUNDING

National Science Foundation CAREER award [MCB 0953714]; National Institutes of Health [R01GM093278]; Burroughs Wellcome Fund Investigator in the Pathogenesis of Infectious Disease award [1015487]; Advanced Photon Source, a U.S. Department of Energy (DOE) Office of Science User Facility operated for the DOE Office of Science by Argonne National Laboratory [DE-AC02-06CH11357]; NE-CAT beamlines, which are funded by the NIGMS from the NIH [P41 GM103403]; SER-CAT beamline; The Pilatus 6M detector on 24-ID-C beam line is funded by a NIH-ORIP HEI grant [S10 RR029205]. Funding for open access charge: Burroughs Wellcome Fund.

Conflict of interest statement. None declared.

REFERENCES

1. Richter,K., Haslbeck,M. and Buchner,J. (2010) The heat shock response: life on the verge of death. *Mol. Cell*, **40**, 253–266.
2. Boutte,C.C. and Crosson,S. (2013) Bacterial lifestyle shapes stringent response activation. *Trends Microbiol.*, **21**, 174–180.
3. Kreuzer,K.N. (2013) DNA damage responses in prokaryotes: regulating gene expression, modulating growth patterns, and manipulating replication forks. *Cold Spring Harbor Perspect. Biol.*, **5**, a012674.
4. Starosta,A.L., Lassak,J., Jung,K. and Wilson,D.N. (2014) The bacterial translation stress response. *FEMS Microbiol. Rev.*, **38**, 1172–1201.
5. Hiraga,S., Jaffe,A., Ogura,T., Mori,H. and Takahashi,H. (1986) F plasmid ccd mechanism in Escherichia coli. *J. Bacteriol.*, **166**, 100–104.
6. Gerdes,K., Rasmussen,P.B. and Molin,S. (1986) Unique type of plasmid maintenance function: postsegregational killing of plasmid-free cells. *Proc. Natl. Acad. Sci. U.S.A.*, **83**, 3116–3120.
7. Gerdes,K., Poulsen,L.K., Thisted,T., Nielsen,A.K., Martinussen,J. and Andreasen,P.H. (1990) The hok killer gene family in gram-negative bacteria. *New Biol.*, **2**, 946–956.
8. Christensen,S.K., Mikkelsen,M., Pedersen,K. and Gerdes,K. (2001) RelE, a global inhibitor of translation, is activated during nutritional stress. *Proc. Natl. Acad. Sci. U.S.A.*, **98**, 14328–14333.
9. Christensen,S.K. and Gerdes,K. (2003) RelE toxins from bacteria and Archaea cleave mRNAs on translating ribosomes, which are rescued by tmRNA. *Mol. Microbiol.*, **48**, 1389–1400.
10. Norton,J.P. and Mulvey,M.A. (2012) Toxin-antitoxin systems are important for niche-specific colonization and stress resistance of uropathogenic Escherichia coli. *PLoS Pathog.*, **8**, e1002954.
11. Helaine,S., Cheverton,A.M., Watson,K.G., Faure,L.M., Matthews,S.A. and Holden,D.W. (2014) Internalization of Salmonella by macrophages induces formation of nonreplicating persisters. *Science*, **343**, 204–208.
12. Page,R. and Peti,W. (2016) Toxin-antitoxin systems in bacterial growth arrest and persistence. *Nat. Chem. Biol.*, **12**, 208–214.
13. Pandey,D.P. and Gerdes,K. (2005) Toxin-antitoxin loci are highly abundant in free-living but lost from host-associated prokaryotes. *Nucleic Acids Res.*, **33**, 966–976.
14. Afif,H., Allali,N., Couturier,M. and Van Melderen,L. (2001) The ratio between CcdA and CcdB modulates the transcriptional repression of the ccd poison-antidote system. *Mol. Microbiol.*, **41**, 73–82.

15. Overgaard,M., Borch,J., Jorgensen,M.G. and Gerdes,K. (2008) Messenger RNA interferase RelE controls relBE transcription by conditional cooperativity. *Mol. Microbiol.*, **69**, 841–857.
16. Garcia-Pino,A., Balasubramanian,S., Wyns,L., Gazit,E., De Greve,H., Magnuson,R.D., Charlier,D., van Nuland,N.A. and Loris,R. (2010) Allostery and intrinsic disorder mediate transcription regulation by conditional cooperativity. *Cell*, **142**, 101–111.
17. Bernard,P. and Couturier,M. (1992) Cell killing by the F plasmid CcdB protein involves poisoning of DNA-topoisomerase II complexes. *J. Mol. Biol.*, **226**, 735–745.
18. Jiang,Y., Pogliano,J., Helinski,D.R. and Konieczny,I. (2002) ParE toxin encoded by the broad-host-range plasmid RK2 is an inhibitor of Escherichia coli gyrase. *Mol. Microbiol.*, **44**, 971–979.
19. Zhang,Y., Zhang,J., Hoeflich,K.P., Ikura,M., Qing,G. and Inouye,M. (2003) MazF cleaves cellular mRNAs specifically at ACA to block protein synthesis in Escherichia coli. *Mol. Cell*, **12**, 913–923.
20. Pedersen,K., Zavialov,A.V., Pavlov,M.Y., Elf,J., Gerdes,K. and Ehrenberg,M. (2003) The bacterial toxin RelE displays codon-specific cleavage of mRNAs in the ribosomal A site. *Cell*, **112**, 131–140.
21. Zhang,Y., Zhang,J., Hara,H., Kato,I. and Inouye,M. (2005) Insights into the mRNA cleavage mechanism by MazF, an mRNA interferase. *J. Biol. Chem.*, **280**, 3143–3150.
22. Jorgensen,M.G., Pandey,D.P., Jaskolska,M. and Gerdes,K. (2009) HicA of Escherichia coli defines a novel family of translation-independent mRNA interferases in bacteria and archaea. *J. Bacteriol.*, **191**, 1191–1199.
23. Christensen-Dalsgaard,M., Jorgensen,M.G. and Gerdes,K. (2010) Three new RelE-homologous mRNA interferases of Escherichia coli differentially induced by environmental stresses. *Mol. Microbiol.*, **75**, 333–348.
24. Winther,K.S. and Gerdes,K. (2011) Enteric virulence associated protein VapC inhibits translation by cleavage of initiator tRNA. *Proc. Natl. Acad. Sci. U.S.A.*, **108**, 7403–7407.
25. Winther,K.S., Brodersen,D.E., Brown,A.K. and Gerdes,K. (2013) VapC20 of Mycobacterium tuberculosis cleaves the Sarcin-Ricin loop of 23S rRNA. *Nat. Commun.*, **4**, 2796.
26. Germain,E., Castro-Roa,D., Zenkin,N. and Gerdes,K. (2013) Molecular mechanism of bacterial persistence by HipA. *Mol. Cell*, **52**, 248–254.
27. Castro-Roa,D., Garcia-Pino,A., De Gieter,S., van Nuland,N.A., Loris,R. and Zenkin,N. (2013) The Fic protein Doc uses an inverted substrate to phosphorylate and inactivate EF-Tu. *Nat. Chem. Biol.*, **9**, 811–817.
28. Cruz,J.W., Rothenbacher,F.P., Maehigashi,T., Lane,W.S., Dunham,C.M. and Woychik,N.A. (2014) Doc toxin is a kinase that inactivates elongation factor Tu. *J. Biol. Chem.*, **289**, 19276.
29. Cheverton,A.M., Gollan,B., Przydacz,M., Wong,C.T., Mylona,A., Hare,S.A. and Helaine,S. (2016) A Salmonella Toxin Promotes Persister Formation through Acetylation of tRNA. *Mol. Cell*, **63**, 86–96.
30. Wilcox,B., Osterman,I., Serebryakova,M., Lukyanov,D., Komarova,E., Gollan,B., Morozova,N., Wolf,Y.I., Makarova,K.S., Helaine,S. *et al.* (2018) Escherichia coli ItaT is a type II toxin that inhibits translation by acetylating isoleucyl-tRNAIle. *Nucleic Acids Res.*, **46**, 7873–7885.
31. Harms,A., Brodersen,D.E., Mitarai,N. and Gerdes,K. (2018) Toxins, targets, and triggers: An overview of toxin-antitoxin biology. *Mol. Cell*, **70**, 768–784.
32. Kamada,K. and Hanaoka,F. (2005) Conformational change in the catalytic site of the ribonuclease YoeB toxin by YefM antitoxin. *Mol. Cell*, **19**, 497–509.
33. Neubauer,C., Gao,Y.G., Andersen,K.R., Dunham,C.M., Kelley,A.C., Hentschel,J., Gerdes,K., Ramakrishnan,V. and Brodersen,D.E. (2009) The structural basis for mRNA recognition and cleavage by the ribosome-dependent endonuclease RelE. *Cell*, **139**, 1084–1095.
34. Heaton,B.E., Herrou,J., Blackwell,A.E., Wysocki,V.H. and Crosson,S. (2012) Molecular structure and function of the novel BrnT/BrnA toxin-antitoxin system of Brucella abortus. *J. Biol. Chem.*, **287**, 12098–12110.
35. Schureck,M.A., Maehigashi,T., Miles,S.J., Marquez,J., Cho,S.E., Erdman,R. and Dunham,C.M. (2014) Structure of the Proteus vulgaris HigB-(HigA)2-HigB toxin-antitoxin complex. *J. Biol. Chem.*, **289**, 1060–1070.
36. Ruangprasert,A., Maehigashi,T., Miles,S.J., Giridharan,N., Liu,J.X. and Dunham,C.M. (2014) Mechanisms of toxin inhibition and transcriptional repression by Escherichia coli DinJ-YafQ. *J. Biol. Chem.*, **289**, 20559–20569.
37. Prysak,M.H., Mozdzierz,C.J., Cook,A.M., Zhu,L., Zhang,Y., Inouye,M. and Woychik,N.A. (2009) Bacterial toxin YafQ is an endoribonuclease that associates with the ribosome and blocks translation elongation through sequence-specific and frame-dependent mRNA cleavage. *Mol. Microbiol.*, **71**, 1071–1087.
38. Hurley,J.M. and Woychik,N.A. (2009) Bacterial toxin HigB associates with ribosomes and mediates translation-dependent mRNA cleavage at A-rich sites. *J. Biol. Chem.*, **284**, 18605–18613.
39. Zhang,Y. and Inouye,M. (2009) The inhibitory mechanism of protein synthesis by YoeB, an Escherichia coli toxin. *J. Biol. Chem.*, **284**, 6627–6638.
40. Maehigashi,T., Ruangprasert,A., Miles,S.J. and Dunham,C.M. (2015) Molecular basis of ribosome recognition and mRNA hydrolysis by the E. coli YafQ toxin. *Nucleic Acids Res.*, **43**, 8002–8012.
41. Schureck,M.A., Dunkle,J.A., Maehigashi,T., Miles,S.J. and Dunham,C.M. (2015) Defining the mRNA recognition signature of a bacterial toxin protein. *Proc. Natl. Acad. Sci. U.S.A.*, **112**, 13862–13867.
42. Schureck,M.A., Maehigashi,T., Miles,S.J., Marquez,J. and Dunham,C.M. (2016) mRNA bound to the 30S subunit is a HigB toxin substrate. *RNA*, **22**, 1261–1270.
43. Hurley,J.M., Cruz,J.W., Ouyang,M. and Woychik,N.A. (2011) Bacterial toxin RelE mediates frequent codon-independent mRNA cleavage from the 5′ end of coding regions in vivo. *J. Biol. Chem.*, **286**, 14770–14778.
44. Christensen-Dalsgaard,M. and Gerdes,K. (2008) Translation affects YoeB and MazF messenger RNA interferase activities by different mechanisms. *Nucleic Acids Res.*, **36**, 6472–6481.
45. Christensen,S.K., Maenhaut-Michel,G., Mine,N., Gottesman,S., Gerdes,K. and Van Melderen,L. (2004) Overproduction of the Lon protease triggers inhibition of translation in Escherichia coli: involvement of the yefM-yoeB toxin-antitoxin system. *Mol. Microbiol.*, **51**, 1705–1717.
46. Feng,S., Chen,Y., Kamada,K., Wang,H., Tang,K., Wang,M. and Gao,Y.G. (2013) YoeB-ribosome structure: a canonical RNase that requires the ribosome for its specific activity. *Nucleic Acids Res.*, **41**, 9549–9556.
47. Janssen,B.D., Garza-Sanchez,F. and Hayes,C.S. (2015) YoeB toxin is activated during thermal stress. *Microbiologyopen*, **4**, 682–697.
48. Clemons,W.M. Jr, Brodersen,D.E., McCutcheon,J.P., May,J.L., Carter,A.P., Morgan-Warren,R.J., Wimberly,B.T. and Ramakrishnan,V. (2001) Crystal structure of the 30 S ribosomal subunit from Thermus thermophilus: purification, crystallization and structure determination. *J. Mol. Biol.*, **310**, 827–843.
49. Selmer,M., Dunham,C.M., Murphy,F.V.t., Weixlbaumer,A., Petry,S., Kelley,A.C., Weir,J.R. and Ramakrishnan,V. (2006) Structure of the 70S ribosome complexed with mRNA and tRNA. *Science*, **313**, 1935–1942.
50. Kabsch,W. (2010) Xds. *Acta Crystallogr.*, **66**, 125–132.
51. Adams,P.D., Afonine,P.V., Bunkoczi,G., Chen,V.B., Davis,I.W., Echols,N., Headd,J.J., Hung,L.W., Kapral,G.J., Grosse-Kunstleve,R.W. *et al.* (2010) PHENIX: a comprehensive Python-based system for macromolecular structure solution. *Acta Crystallogr.*, **66**, 213–221.
52. Emsley,P., Lohkamp,B., Scott,W.G. and Cowtan,K. (2010) Features and development of Coot. *Acta Crystallogr.*, **66**, 486–501.
53. Wimberly,B.T., Brodersen,D.E., Clemons,W.M. Jr, Morgan-Warren,R.J., Carter,A.P., Vonrhein,C., Hartsch,T. and Ramakrishnan,V. (2000) Structure of the 30S ribosomal subunit. *Nature*, **407**, 327–339.
54. Painter,J. and Merritt,E.A. (2006) Optimal description of a protein structure in terms of multiple groups undergoing TLS motion. *Acta Crystallogr.*, **62**, 439–450.
55. Jenner,L.B., Demeshkina,N., Yusupova,G. and Yusupov,M. (2010) Structural aspects of messenger RNA reading frame maintenance by the ribosome. *Nat. Struct. Mol. Biol.*, **17**, 555–560.

56. Cruz-Reyes,J., Piller,K.J., Rusche,L.N., Mukherjee,M. and Sollner-Webb,B. (1998) Unexpected electrophoretic migration of RNA with different 3′ termini causes a RNA sizing ambiguity that can be resolved using nuclease P1-generated sequencing ladders. *Biochemistry*, **37**, 6059–6064.
57. Ogle,J.M., Murphy,F.V., Tarry,M.J. and Ramakrishnan,V. (2002) Selection of tRNA by the ribosome requires a transition from an open to a closed form. *Cell*, **111**, 721–732.
58. Ying,L. and Fredrick,K. (2016) Epistasis analysis of 16S rRNA ram mutations helps define the conformational dynamics of the ribosome that influence decoding. *RNA*, **22**, 499–505.
59. Hoffer,E.D., Maehigashi,T., Fredrick,K. and Dunham,C.M. (2018) Ribosomal ambiguity (ram) mutations promote the open (off) to closed (on) transition and thereby increase miscoding. *Nucleic Acids Res.*, **47**, 1557–1563.
60. Schureck,M.A., Repack,A., Miles,S.J., Marquez,J. and Dunham,C.M. (2016) Mechanism of endonuclease cleavage by the HigB toxin. *Nucleic Acids Res.*, **44**, 7944–7953.
61. Schifano,J.M., Edifor,R., Sharp,J.D., Ouyang,M., Konkimalla,A., Husson,R.N. and Woychik,N.A. (2013) Mycobacterial toxin MazF-mt6 inhibits translation through cleavage of 23S rRNA at the ribosomal A site. *Proc. Natl. Acad. Sci. U.S.A.*, **110**, 8501–8506.
62. Schifano,J.M., Vvedenskaya,I.O., Knoblauch,J.G., Ouyang,M., Nickels,B.E. and Woychik,N.A. (2014) An RNA-seq method for defining endoribonuclease cleavage specificity identifies dual rRNA substrates for toxin MazF-mt3. *Nat. Commun.*, **5**, 3538.
63. Hoffer,E.D., Miles,S.J. and Dunham,C.M. (2017) The structure and function of Mycobacterium tuberculosis MazF-mt6 toxin provide insights into conserved features of MazF endonucleases. *J. Biol. Chem.*, **292**, 7718–7726.
64. Culviner,P.H. and Laub,M.T. (2018) Global Analysis of the E. coli Toxin MazF Reveals Widespread Cleavage of mRNA and the Inhibition of rRNA Maturation and Ribosome Biogenesis. *Mol. Cell*, **70**, 868–880.
65. Tian,Q.B., Ohnishi,M., Tabuchi,A. and Terawaki,Y. (1996) A new plasmid-encoded proteic killer gene system: cloning, sequencing, and analyzing hig locus of plasmid Rts1. *Biochem. Biophys. Res. Commun.*, **220**, 280–284.